catalysts

MDPI

Supplementary materials

The Impact of Functionality and Porous System of Nanostructured Carriers Based on Metal–Organic Frameworks of UiO-66-Type on Catalytic Performance of Embedded Au Nanoparticles in Hydroamination Reaction

Vera I. Isaeva, Vladimir V. Chernyshev, Vadim V. Vergun, Danil A. Arkhipov, Grigory S. Deyko, Lev M. Glukhov, Gennady I. Kapustin, Olga P. Tkachenko and Leonid M. Kustov

1. Textural properties of theAu@meso-UiO-66-before-catalysis, Au@meso-NH_2-UiO-66-before-catalysis and Au@meso-NH_2-UiO-66-after-catalysis nanohybrids

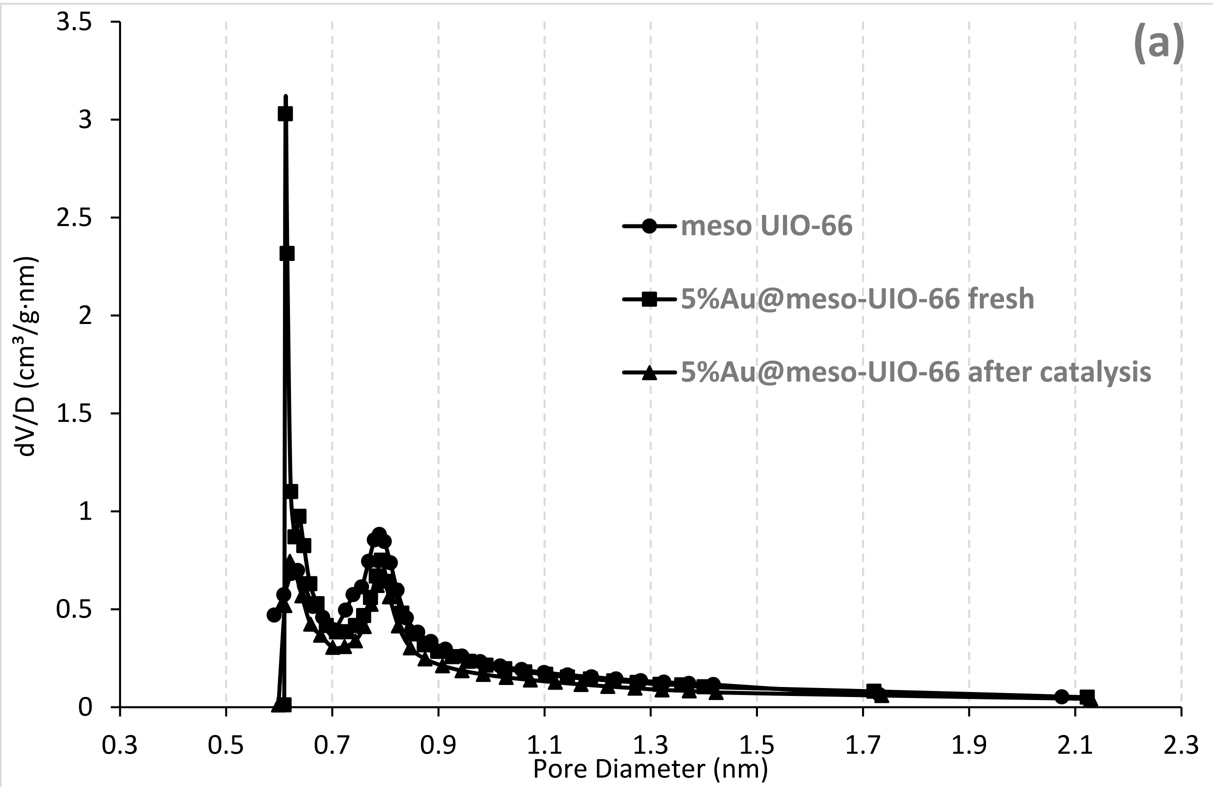

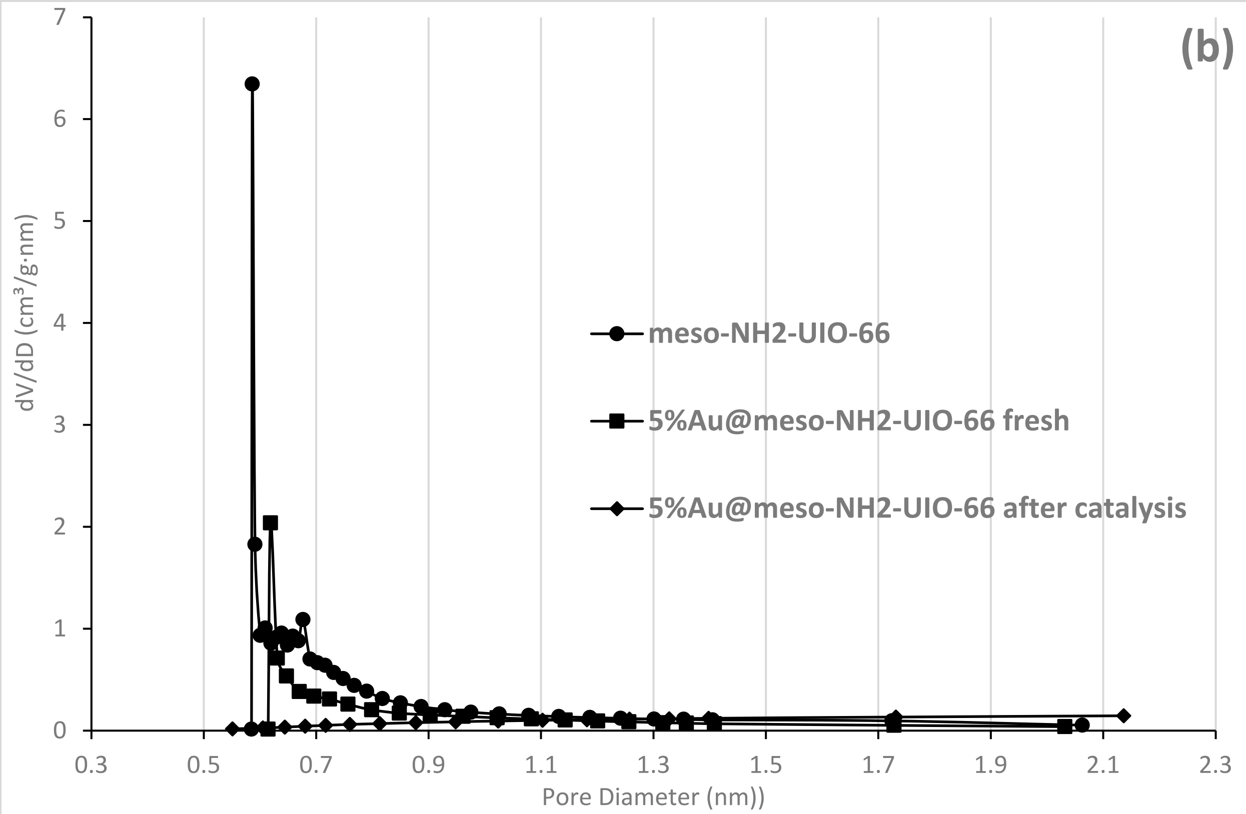

Figure S1. Micropore size distribution calculated by the Horwath-Kawazoe method in assumption of a cylinder pore geometry (Saito-Foley).(**a**)—meso-UiO-66 and Au@meso-UiO-66-before- and -after-catalysis materials; (**b**)—meso-NH_2-UiO-66 and Au@meso-NH_2-UiO-66-before- and -after-catalysis materials.

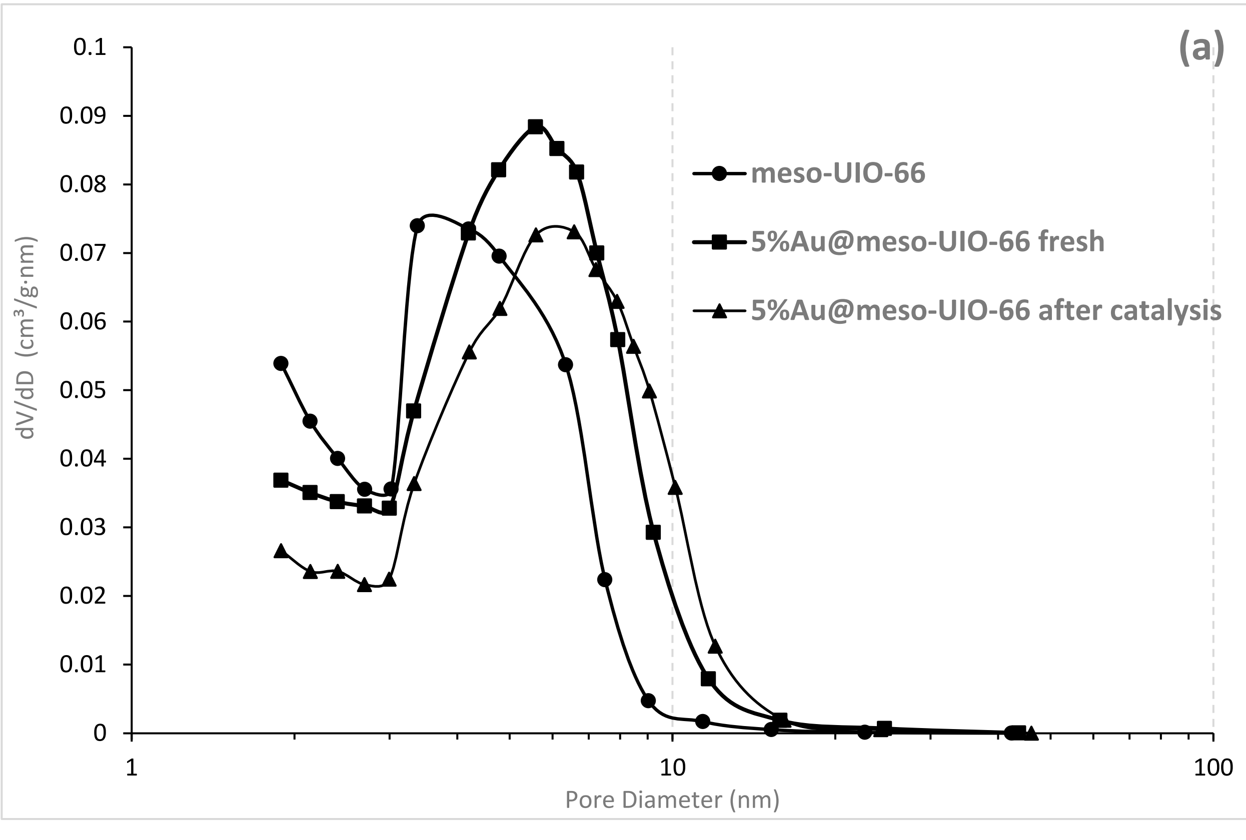

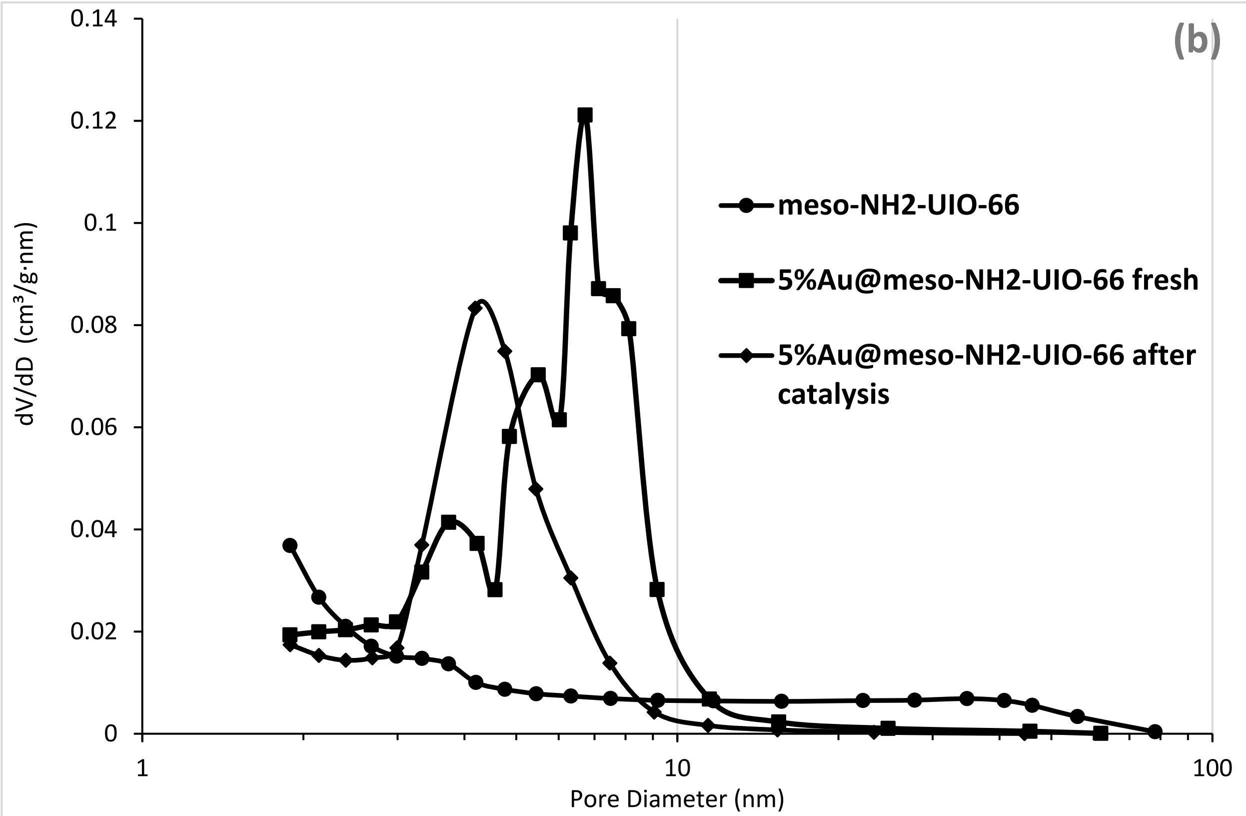

Figure S2.Mesopore size distribution calculated by the BJH method. (**a**)—meso-UiO-66 and Au@meso-UiO-66-before- and -after-catalysis materials; (**b**)—meso-NH_2-UiO-66 and Au@meso-NH_2-UiO-66-before- and -after-catalysis materials.

2. Gold content in theAu@meso-UiO-66 and Au@meso-NH_2-UiO-66 nanohybrids

Table S1. Gold content (wt.%) in theAu@meso-UiO-66 and Au@meso-NH_2-UiO-66-before- and -after-catalysis nanohybrids.

Element	Au@meso-UiO-66-before-catalysis	Au@meso-UiO-66-after-catalysis	Au@meso-NH_2-UiO-66-before-catalysis	Au@meso-NH_2-UiO-66-after-catalysis
Au, mass %	3.34	3.06	2.14	1.96

3.Au-NP distribution on sizes in the Au@meso-UiO-66-before-catalysis, Au@meso-UiO-66-after-catalysis, Au@meso-NH_2-UiO-66-before-catalysis and Au@meso-NH_2-UiO-66-after-catalysis nanohybrids

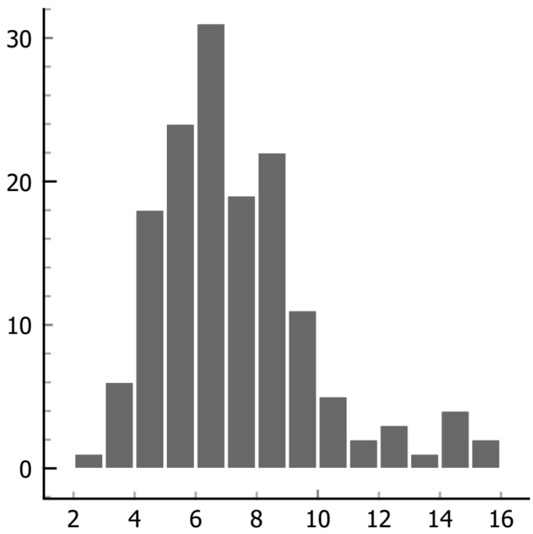

Figure S3. Au-NP distribution on sizes for the Au@meso-UiO-66-before-catalysis nanohybrid.

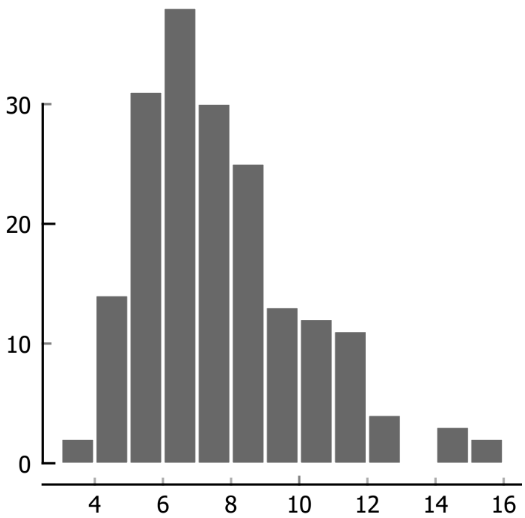

Figure S4. Au-NP distribution on sizes for the Au@meso-NH_2-UiO-66-before-catalysis nanohybrid.

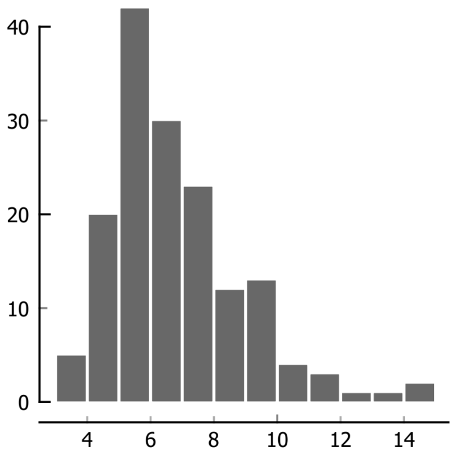

Figure S5. Au-NP distribution on sizes for the Au@meso-UiO-66-after-catalysis nanohybrid.

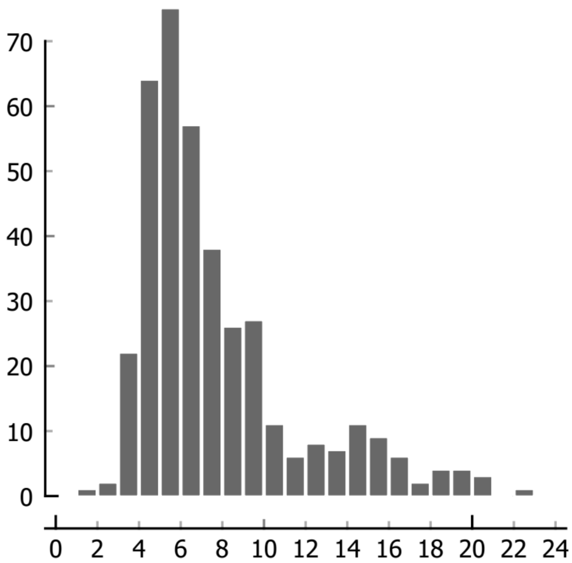

Figure S6. Au-NP distribution on sizes for the Au@meso-NH_2-UiO-66-after-catalysis nanohybrid.

4. DRIFT spectra of the meso-UiO-66 and meso-NH_2-UiO-66 carriers

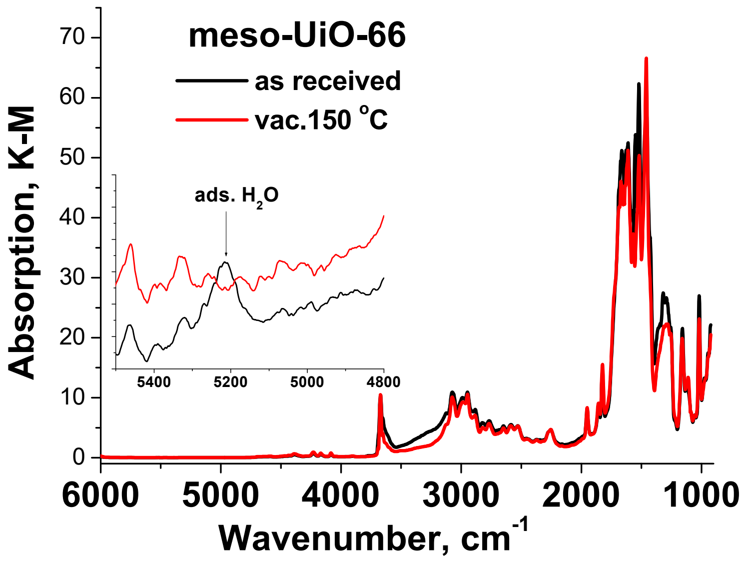

Figure S7.DRIFT spectra of both meso-UiO-66 samples before (as received) and after treatment in vacuum at 150 °C in full scale.

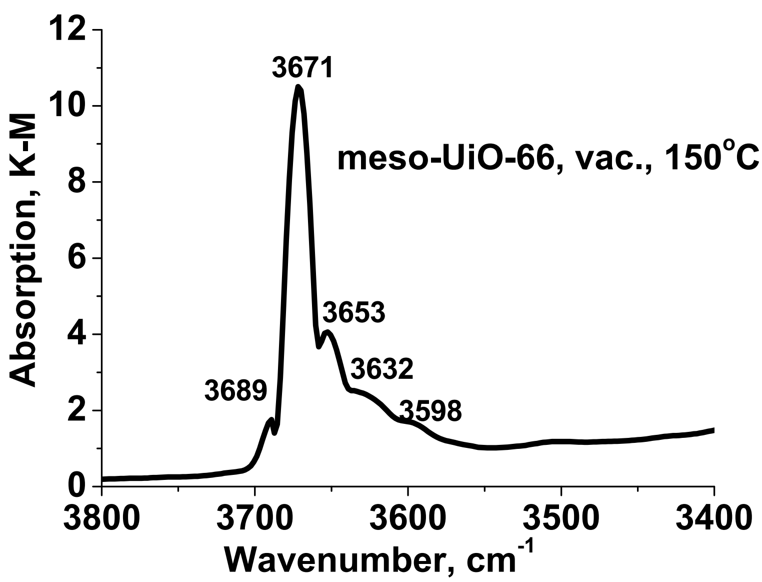

Figure S8. DRIFT spectrum of meso-UiO-66 sample after evacuation in the region of 3800–3400 cm^{-1}.

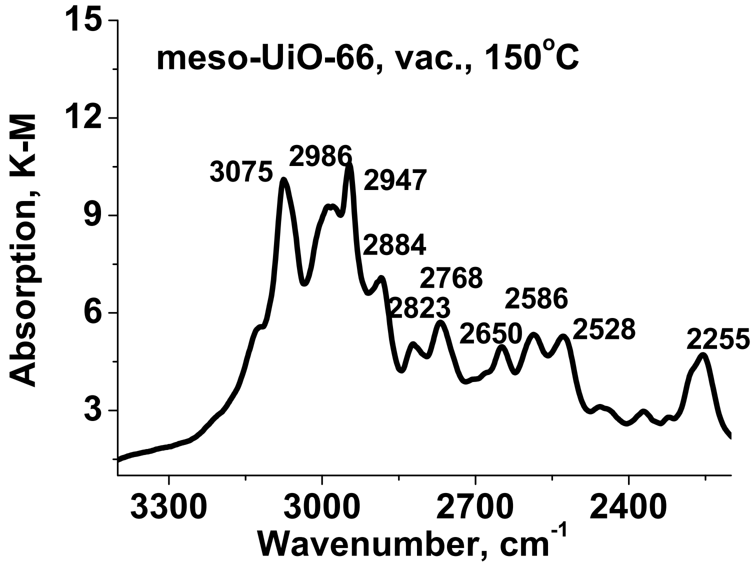

Figure S9. DRIFT spectrum of meso-UiO-66 sample after evacuation in the region of 3400–2200 cm^{-1}.

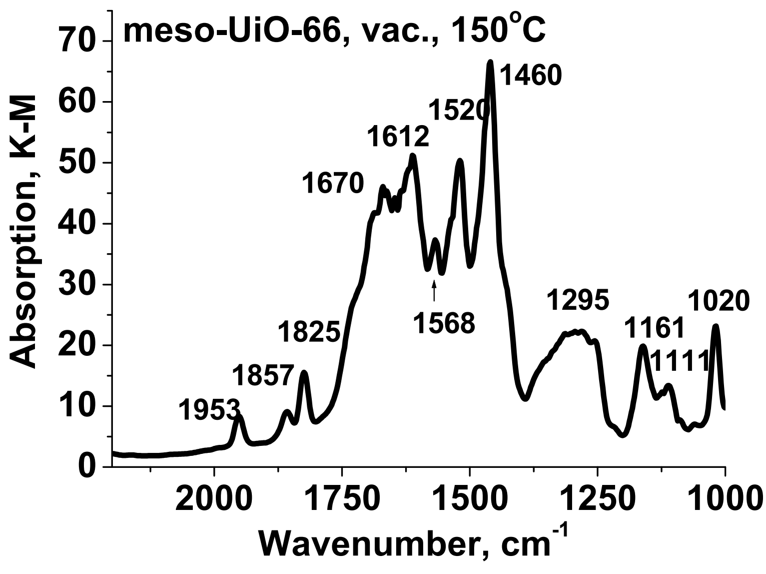

Figure S10. DRIFT spectrum of meso-UiO-66 sample after evacuation in the region of 2200–1000 cm^{-1}.

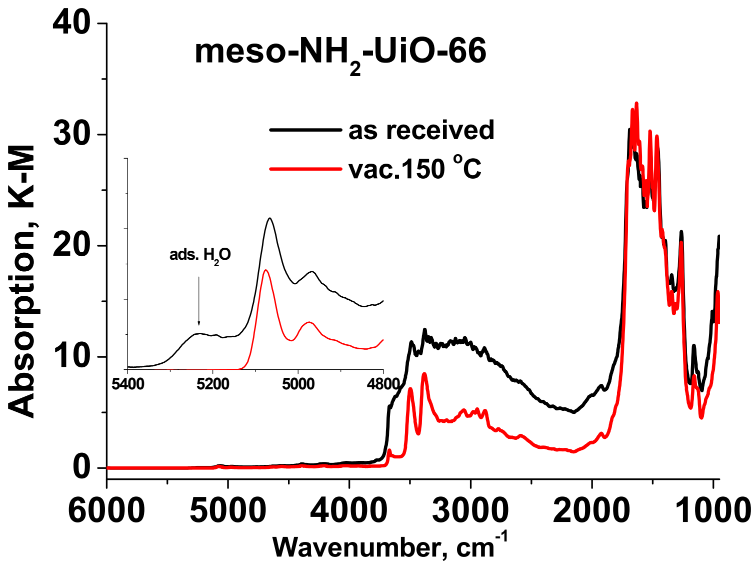

Figure S11. DRIFT spectra of both meso-NH$_2$-UiO-66 samples before (as received) and after treatment in vacuum at 150 °C in full scale.

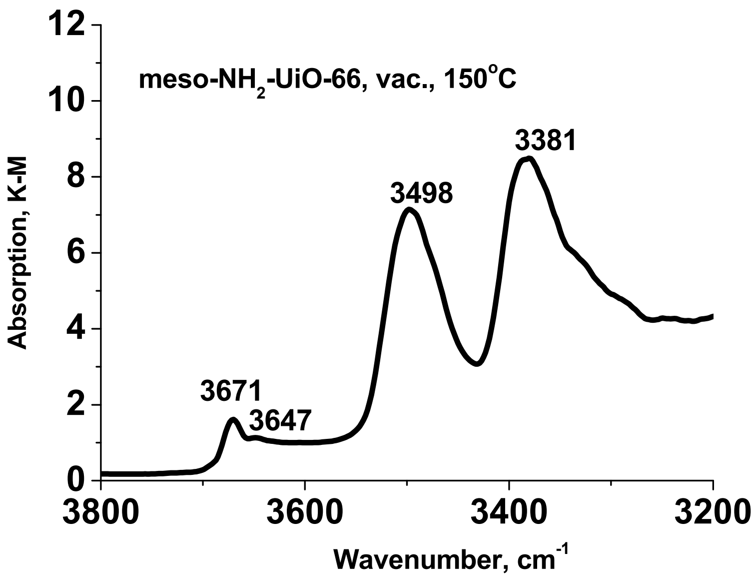

Figure S12. DRIFT spectrum of meso-NH$_2$-UiO-66 sample after evacuation in the region of 3800–3200 cm^{-1}.

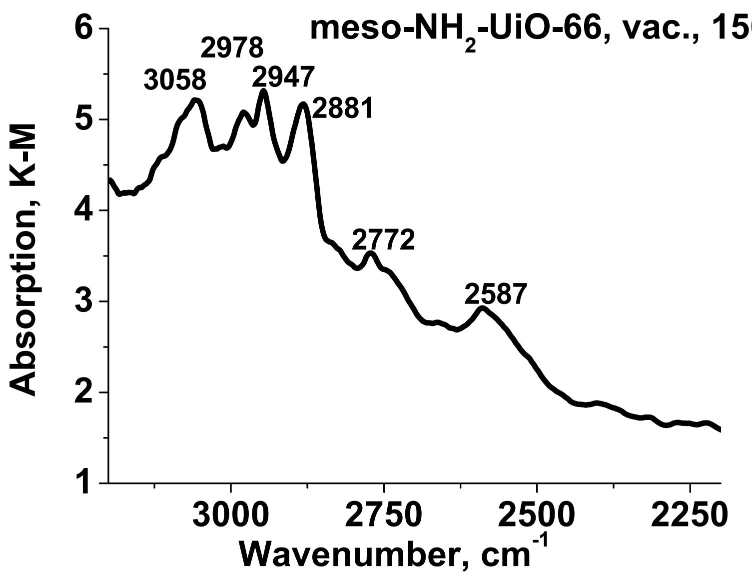

Figure S13. DRIFT spectrum of meso-NH_2-UiO-66 sample after evacuation in the region of 3200–2200 cm^{-1}.

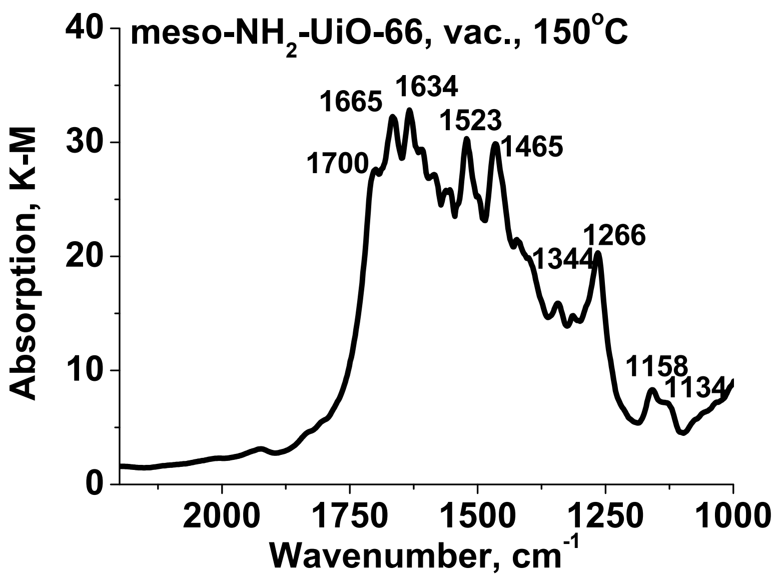

Figure S14. DRIFT spectrum of meso-NH_2-UiO-66 sample after evacuation in the region of 2200–1000 cm^{-1}.

5. DRIFT spectra of adsorbed CD_3CN at room temperature on meso-UiO-66 and meso-NH_2-UiO-66 materials

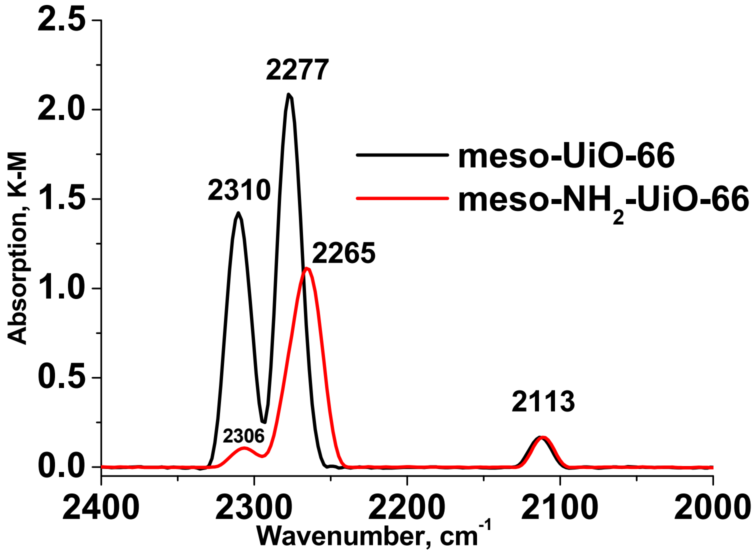

Figure S15. DRIFT spectra of adsorbed CD_3CN at room temperature on meso-UiO-66 and meso-NH_2-UiO-66 samples.

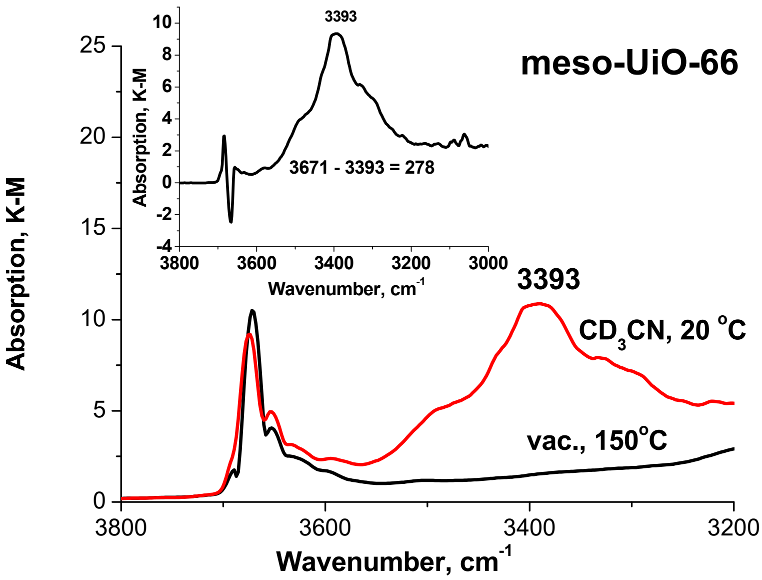

Figure S16. The comparison of DRIFT spectra before and after CD_3CN adsorption on meso-UiO-66 material.

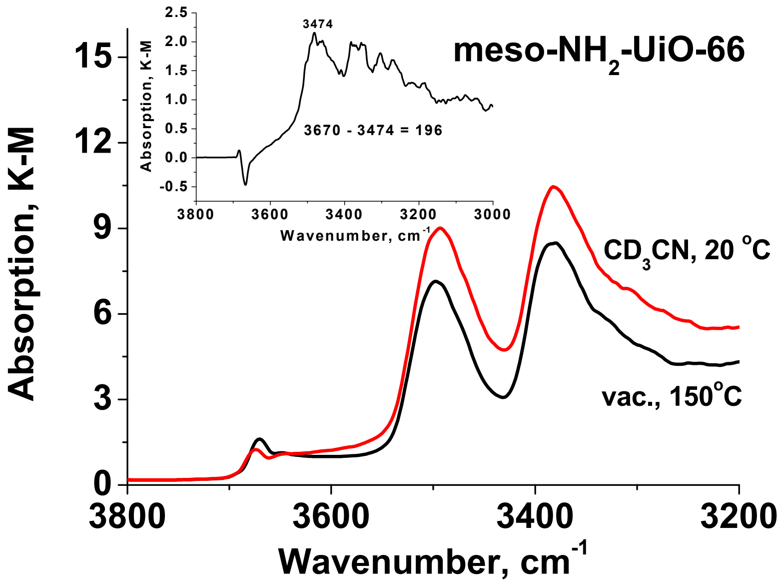

Figure S17. The comparison of DRIFT spectra before and after CD_3CN adsorptionon meso-UiO-66 material.

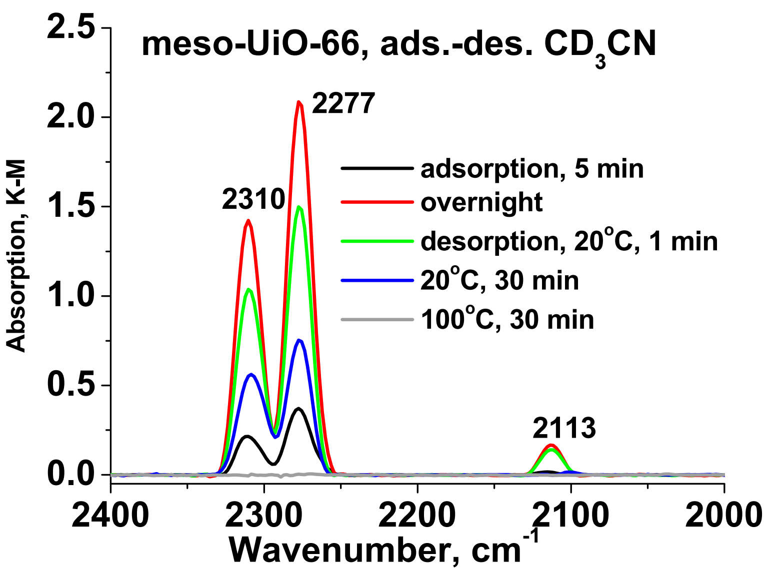

Figure S18. DRIFT-CD_3CN spectra in adsorption-desorption process on meso-UiO-66 material.

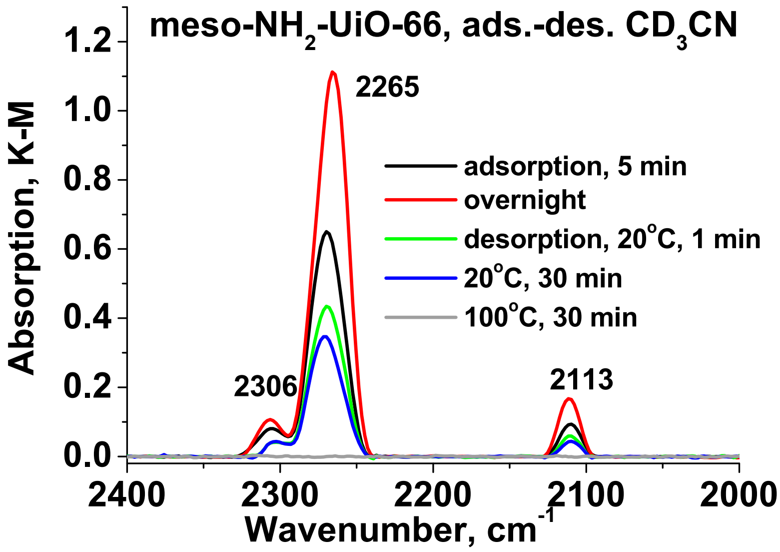

Figure S19. DRIFT-CD_3CN spectra in adsorption-desorption process on meso-NH_2-UiO-66 sample.

6. TGA examinations of the micro-UiO-66 and meso-UiO-66 materials.

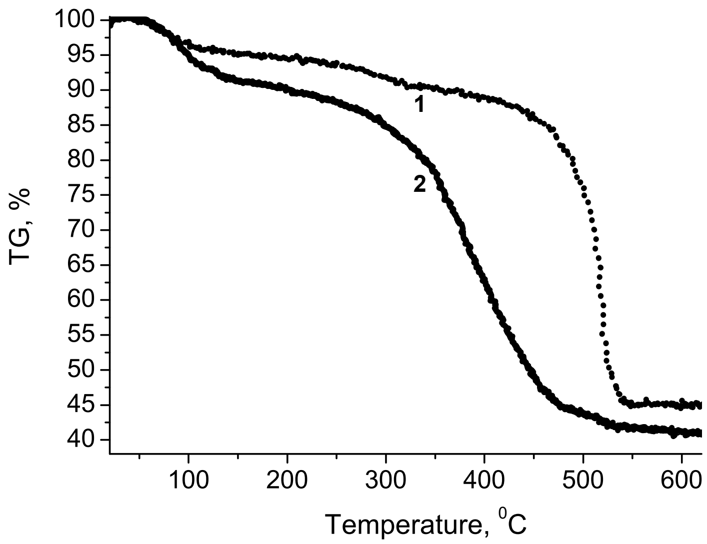

Figure S20. TGA curves for the meso-UiO-66 (**1**) and micro-UiO-66 (**2**) samples.

Table S2. The evaluation of the number of missing linkers per hexa-nuclear zirconium node and deficiency extent in the micro-UiO-66 and meso-UiO-66 materials.

Material	Number of missing linkers per Zr_6O_6 node	Deficiency extent, %
micro-UiO-66	0.47 ± 0.28	7.8 ± 4.7
meso-UiO-66	1.54 ± 0.24	25 ± 4.0

7. Hydroamination of phenylacetylene with aniline over Au@meso-NH$_2$-UiO-66 nanocatalyst in the toluene medium

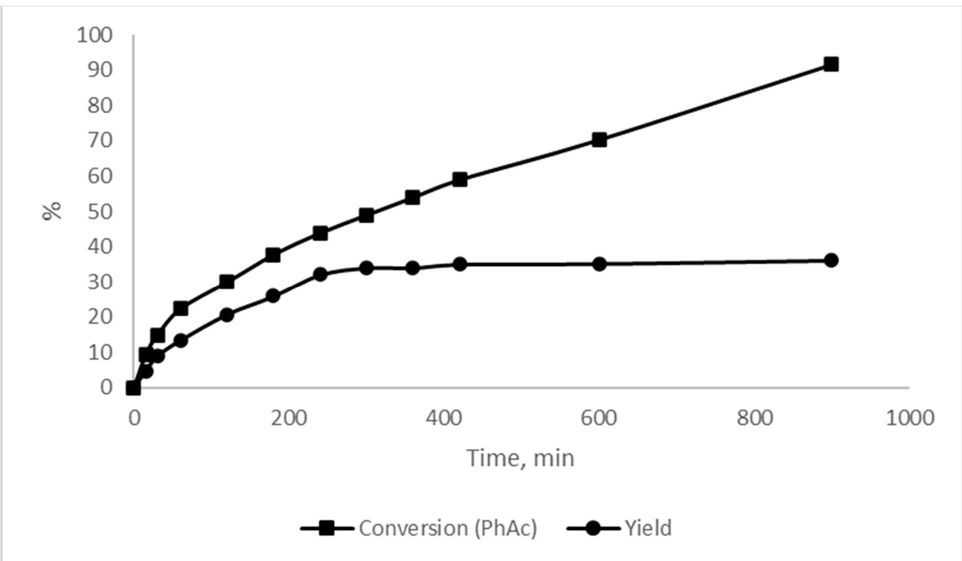

Figure S21. Hydroamination of phenylacetylene with aniline over Au@meso-NH$_2$-UiO-66 nanohybrid; toluene used as solvent. The Au content in the catalyst is 2.14 wt.%.